

On the calculation of normals in free-surface flow problems

M.A. Walkley^{1,*}, P.H. Gaskell², P.K. Jimack¹, M.A. Kelmanson³,
J.L. Summers² and M.C.T. Wilson²

¹ *School of Computing, University of Leeds, Leeds, LS2 9JT, UK*

² *School of Mechanical Engineering, University of Leeds, Leeds, LS2 9JT, UK*

³ *Department of Applied Mathematics, University of Leeds, Leeds, LS2 9JT, UK*

SUMMARY

The use of boundary-conforming finite-element methods is considered for the solution of surface-tension-dominated free-surface flow problems in three dimensions. This class of method is based upon the use of a moving mesh whose velocity is driven by the motion of the free surface, which is in turn determined via a kinematic boundary condition for the normal velocity. The significance of the method used to compute the normal direction at the finite-element node points for a C^0 piecewise-polynomial free surface is investigated. In particular, it is demonstrated that the concept of mass-consistent normals on an isoparametric quadratic tetrahedral mesh is flawed. In this case an alternative, purely geometric, normal is shown to lead to a far more robust numerical algorithm. Copyright © 2003 John Wiley & Sons, Ltd.

KEY WORDS: Finite element method; Free surface flow; Surface tension; Normals

1. INTRODUCTION

Free-surface flow problems are of great importance in the modelling of a wide range of physical phenomena, from phase-change problems [1, 2] through to coating flows [3, 4], sintering [5, 6] or the

*Correspondence to: M.A. Walkley, School of Computing, University of Leeds, Leeds, LS2 9JT, UK.

Email: markw@comp.leeds.ac.uk

Contract/grant sponsor: EPSRC; contract/grant number: GR/R25453/01

spreading of viscous fluids [7, 8]. In two dimensions, computational fluid dynamics (CFD) techniques for solving time-dependent free-surface problems are becoming well established [6, 9, 10] and, in three dimensions, there has been a significant amount of important recent research [2, 11, 12, 13]. One of the most popular classes of methods in both two and three dimensions is based upon the use of boundary-conforming moving/adapting meshes, as in the arbitrary Lagrangian-Eulerian (ALE) finite element method. Other techniques include Eulerian algorithms such as the volume-of-fluid method [14, 15]. In such methods a larger domain is required than the region occupied by a single fluid and the interface is reconstructed in some manner, usually through the use of a characteristic or auxiliary function. In order to maintain accuracy with this approach, considerable local mesh refinement is required to track the free surface. Conversely, purely Lagrangian algorithms have also been developed, such as those described in [16, 17]. These too have the potential to be highly accurate but often at the expense of frequent remeshing. In this paper, however, attention is restricted to ALE algorithms in which the mesh conforms to the dynamic free surface at all times.

One of the main advantages of boundary-conforming ALE algorithms is their potential to represent the moving free surface to a very high accuracy. Surface-tension effects couple the geometry of the free surface to its motion, which in turn induces flow effects in the bulk fluid. Hence the ability to accurately model the geometry and the kinematics of the free surface is generally of great importance. Usually, the representation of the surface takes the form of a C^0 piecewise polynomial whose accuracy can be maintained through the use of local mesh refinement as the solution—and therefore the boundary—evolves. A significant amount of work has been undertaken in both two and three dimensions using this approach. Examples include, but are not limited to, the work of Cairncross *et al.* [11], Lynch *et al.* [1, 18], Peterson *et al.* [10, 19], Soulaïmani and Saad [12], and Zhou and Derby [13].

In the present paper, a three-dimensional ALE algorithm is presented based on standard isoparametric tetrahedral Taylor-Hood finite elements. This is a generalization of the two-dimensional work of [10, 19]. It is demonstrated that, in the presence of a kinematic boundary condition which stipulates the normal motion of the free surface, the manner in which the normal to the piecewise-polynomial boundary is calculated is of critical importance. In particular, an observation is presented that the use of so-called *mass-consistent* normals [18, 20] is no longer valid for this finite element discretisation in three dimensions, despite being the *de facto* implementation in the two-dimensional algorithm.

2. OVERVIEW OF THE SOLUTION ALGORITHM

The precise ALE algorithm used for this work is an extension of the two-dimensional work in [10] and therefore only a brief overview is provided. It is emphasized, however, that the conclusions of this work are neither specific nor restricted to the precise ALE implementation used herein.

The following non-dimensional form of the incompressible Navier-Stokes equations is considered;

$$Re \left(\frac{\partial \underline{u}}{\partial t} + \underline{u} \cdot \nabla \underline{u} \right) = \nabla \cdot \underline{\sigma} + St \underline{f}, \quad (1)$$

$$\nabla \cdot \underline{u} = 0. \quad (2)$$

Here \underline{u} is velocity, $\underline{\sigma} = -p\mathbf{I} + \nabla \underline{u} + \nabla \underline{u}^T$ is the stress tensor, p is pressure, \mathbf{I} is the identity tensor, Re the Reynolds number, St the Stokes number and \underline{f} the exterior force. At a solid boundary, the no-slip boundary condition is applied and, at a free surface the following kinematic condition and stress condition are applied:

$$\underline{n} \cdot (\underline{u} - \dot{\underline{x}}_{fs}) = 0, \quad (3)$$

$$\underline{n} \cdot \underline{\sigma} = -\underline{n} p_{\text{ext}} + \frac{1}{Ca} (\nabla_S \cdot \underline{n}) \underline{n}. \quad (4)$$

In (3) \underline{n} represents the outward normal to the free surface whose location is given by \underline{x}_{fs} , \underline{u} represents the fluid velocity at a point on the free surface and the dot above a variable denotes its time derivative. In (4) p_{ext} is the external pressure, which may be taken as zero for simplicity, $\nabla_S = (\mathbf{I} - \underline{nn}) \cdot \nabla$ is the surface gradient operator and Ca is the capillary number which is inversely proportional to surface tension (which in the present work is assumed constant over the entire free surface).

The problem is simplified by considering Stokes flows only, for which Re is zero, in the absence of gravity, so that \underline{f} vanishes. Equations (1) and (2) are discretized using an isoparametric Taylor-Hood finite-element method with quadratic velocities and linear pressures on an unstructured tetrahedral mesh, which is known to be stable [20]. On the piecewise-quadratic free surface, the natural boundary condition (4) is imposed weakly, followed by application of the surface divergence theorem. Having obtained an instantaneous velocity field, the kinematic boundary condition (3) is used to determine the instantaneous normal motion on the free surface; note that this step depends critically upon the definition chosen for the normal direction along free-surface edges and at free-surface nodes.

The position of the free surface is updated explicitly using the normal velocity just computed. This has the effect of changing the geometry of the problem domain and so the finite-element mesh also

requires updating at the end of each time step. To achieve this a linear elasticity model, similar to that described in [11], is used. Effectively, the nodes in the mesh are treated as points in a linear elastic material which is deformed by applying a displacement that is equal to the displacement in the free surface over the time step. This uniquely determines the displacement of each point in the mesh in a manner that prevents tangling, at least for moderate free-surface motions. Having updated both the free surface and the mesh, the solution of (1) and (2) may now be computed to obtain the instantaneous velocity field at the start of the next time step.

As indicated in the introduction, there is an important issue associated with the kinematic boundary condition (3) since, for a typical finite-element solution, \underline{n} is not uniquely defined in three dimensions at node points and element edges on the free surface. Numerical techniques such as that described above, however, seek to apply (3) at the nodes on this surface, either explicitly or implicitly, in order to update the boundary location over a time step.

3. COMPUTATION OF THE BOUNDARY NORMALS

There are a number of possible ways in which one may interpret (3) at a finite-element node on the free surface. In the numerical investigations described below, two different choices of normal direction are considered. In particular, the standard mass-consistent normals, used successfully in the two-dimensional algorithm, are shown *not* to generalize to three-dimensional algorithms of the form described in Section 2.

Mass-consistent normals

In [20], results of Engelman *et al.* [21] are described in which the unit normal at node j , \underline{n}_j say, is derived from the discrete weak continuity equation for incompressible flow. After some algebra this yields the expression

$$\underline{n}_j = \frac{\int_{\Gamma} \underline{n} \phi_j ds}{\|\int_{\Gamma} \underline{n} \phi_j ds\|}, \quad (5)$$

where Γ is the free surface and ϕ_j is the finite-element velocity basis function at node j . Note that this expression for the normal is also used by Lynch and Gray [18], although they do not derive it from the view point of mass conservation. In [20], (5) is referred to as the mass-consistent normal. Mass-consistent normals have been used in two-dimensional finite element simulations of free-surface flow

by several authors including the two-dimensional version of the algorithm described in Section 2 [10].

An important observation when seeking to employ (5) at a vertex, j say, is that the expression takes the form of a weighted average normal, with the vertex basis function, ϕ_j , acting as the weight. For three-dimensional quadratic tetrahedral elements this weight is non-positive, and in particular the vertex basis function, ϕ_j , has the property that

$$\int_{\Gamma} \phi_j ds = 0. \quad (6)$$

This is a particularly undesirable property for the computation of the mass-consistent normal. For example, if the mass consistent normal is computed on a plane surface, where the normal is constant, the result will be the zero vector if (5) is used. Even on a curved surface on which the normal varies smoothly on an element, with jump discontinuities between the elements, the property (6) ensures that the quality of the normal computed by (5) will be very poor, being greatly affected by cancellation, and often not at all representative of the local surface geometry. Note that the edge nodes of the quadratic tetrahedral elements are unaffected since the basis functions associated with these nodes are always positive and the mass-consistent normal can be computed reliably at these points.

In the two-dimensional case, when isoparametric quadratic triangular elements are used, the problem does not manifest itself. The vertex basis functions, ϕ_j , are again non-positive but in this case satisfy

$$\int_{\Gamma} \phi_j ds = \frac{1}{6} > 0. \quad (7)$$

As outlined below, this is sufficient to ensure that problems do not occur in two dimensions. Considering a one-dimensional piecewise-quadratic segment of the finite-element domain boundary, depicted in Figure 1, a precise form for the mass-consistent normal (5) can be derived by substitution of the standard quadratic basis functions. The numerator of the mass consistent normal (5) at the vertex, \mathbf{n}_j , can be written as

$$\mathbf{n}_j = \frac{1}{6} ((y_k - y_i) - 4(y_q - y_p), -(x_k - x_i) + 4(x_p - x_q)). \quad (8)$$

Note that if, for example, $(y_k - y_i) = 4(y_q - y_p)$ the x -component of the normal can be made zero, with a similar possibility for the y -component. However, the distortion to the element implied by these equalities occurring simultaneously would be such that the Jacobian of the isoparametric mapping becomes singular. Furthermore, previous work in two dimensions [10, 19] avoids such potential difficulties by automatically maintaining the position of the edge nodes at the centre of the quadratic edge during the mesh movement stage. This was imposed primarily to ensure the Jacobian of the

isoparametric mapping does not become near-to singular, but has the additional effect of ensuring that the mass-consistent normals work as designed in two dimensions.

Arithmetic-average normals

An alternative expression for the normal to a finite-element free surface node may be obtained from purely geometric considerations, i.e. by taking the average normal direction from elements sharing that node. At the general node j , this yields the expression

$$\underline{n}_j = \frac{\frac{1}{N(j)} \sum_{k=1}^{N(j)} \underline{n}(\underline{x}_j)|_{\Omega_j(k)}}{\left\| \frac{1}{N(j)} \sum_{k=1}^{N(j)} \underline{n}(\underline{x}_j)|_{\Omega_j(k)} \right\|}. \quad (9)$$

Here \underline{x}_j is the location of node j , $N(j)$ is the number of free-surface elements sharing node j , $\{\Omega_j(1), \dots, \Omega_j(N(j))\}$ is the set of these elements, and $\underline{n}(\underline{x}_j)|_{\Omega}$ is the limit of $\underline{n}(\underline{x})$ as \underline{x} approaches \underline{x}_j from within the free surface of element Ω . This approach of calculating an arithmetic average of the normal on neighbouring elements has been reported in the three-dimensional work of [11], which uses linear hexahedral elements, though they do not comment on alternative methods for computing the normal.

It is demonstrated in the following section that use of the arithmetic-average normal allows robust computation for some typical three-dimensional free-surface flows and mass is conserved with a high degree of accuracy. The weakness of the mass-consistent approach for quadratic tetrahedral elements is further highlighted, despite its successful use for two-dimensional problems.

4. NUMERICAL RESULTS

Results are presented for the solution of two simple model problems in three dimensions using the algorithm of Section 2. The first problem involves a large induced tangential velocity field on the free surface, with the normal motion of the surface expected to be small. The second problem comprises a large deformation of the fluid surface, and hence significant movement of the free surface as it recovers to its equilibrium state. The spatial domain considered for both problems consists of a thick layer of fluid covering a sphere of unit radius. The numerical model thus consists of a solid-wall interior boundary and a free-surface exterior boundary surrounding the fluid. This domain is discretized using the NETGEN software [22] to produce an unstructured isoparametric quadratic tetrahedral mesh with

719 elements and 1433 nodes. A two-dimensional example is also presented, analogous to the second three-dimensional example, to illustrate the successful use of the mass-consistent normals in this case.

4.1. A rotating spherical core

Fluid is initially distributed in a uniform spherical shell about a central spherical solid core which is rotating with unit angular velocity about the z -axis. This induces a relatively large tangential velocity on the free surface, compared to the normal component. In the absence of gravity and inertial terms no significant normal motion of the free surface is expected. Problems with large tangential velocities are not unrealistic for this type of fluid model, occurring, for example, in studies of the supported load on a rotating cylinder [19].

Figure 2(a)-(b) shows the free surface shape produced when using the arithmetic-average normals. As can be seen, the surface varies imperceptibly from its initial state, since no normal motion is generated by the tangential velocity field. Although the results with the arithmetic-average normals show a steady loss of mass over time, the actual amount is small in relative terms, being approximately $10^{-2}\%$ after 10^4 time steps (a real time of $t=10$, corresponding to $5/\pi$ sphere rotations). Given that the mesh employs only 719 elements, it should be borne in mind that even this small loss of mass may be reduced further by using a finer grid. Figure 2(c) shows the distinctly non-physical nature of the surface produced when mass-consistent normals are used. An equilibrium position is reached that bears no relation to the expected physical result since the computed surface normals are not initially perpendicular to the tangential velocity field. Note, however, that mass is conserved in this case to within $10^{-3}\%$ over the same simulation time.

4.2. Perturbed free surface

In this case a problem is considered in which a large normal motion of the fluid free surface is expected. The free surface of the fluid is stretched along the x -axis by a factor 1.5 into an initially elliptical shape. In the absence of gravity, surface tension will tend to draw the fluid back into a sphere about the inner core.

Using the arithmetic-average normals the solution is computed for 10^4 time steps (a real time of $t=10$) and it evolves smoothly towards the expected spherical shape, as depicted in Figure 3. The volume change during the simulation, even after 10^4 time steps, is only $5 \times 10^{-3}\%$ of the total volume. It is noteworthy that use of the mass-consistent normals in this example caused the algorithm to fail

completely.

4.3. Comparison with two-dimensional simulations

Results from the two-dimensional algorithm have been presented elsewhere [10, 19]. Here a single example is shown employing mass-consistent normals, illustrating their successful use in this case. An annular layer of fluid, surrounding a solid circular internal boundary, is initially stretched into an elliptical shape; in the absence of gravity it returns to the circular equilibrium position under the action of surface tension. Figures 4(a)-(c) show the evolution of the free-surface shape and the maximum velocity magnitude computed on the free surface. During 10^4 time steps (a real time of $t=10$) of the simulation on this relatively coarse mesh mass is conserved to within $2 \times 10^{-4}\%$, emphasising the utility of the mass-consistent normals in this two-dimensional case.

5. CONCLUSIONS

Surface tension is the dominating force for a large class of physical problems, and the accuracy of computational models for such problems therefore depends critically on the accurate representation of the curvature of the fluid free surface, which in turn is used to determine the motion of the free surface.

The mass-consistent normal is derived from the viewpoint of mass conservation and as such appears to work well for many problems. As shown in Section 3 however there is a serious flaw in applying this method to the standard Taylor-Hood tetrahedral finite element method in three dimensions, and while the method will generally work in the two-dimensional case it is necessary to ensure that the edge nodes are constrained to lie close to the midpoint of the edges. The numerical results in Section 4 corroborate these observations.

The arithmetic-average normals described in Section 3 do not have any implicit mass-conservation properties but are accurate in the sense that they are derived from the geometry of the free surface. In practice they always provide a smooth evolution of the free surface and flow field. The results show that, with this choice, the volume of the fluid decreases over time, but the rate of decrease is relatively small, even when using the quite coarse meshes in the examples above. Hence for tetrahedral Taylor-Hood elements these normals are to be preferred.

ACKNOWLEDGEMENTS

The authors wish to thank an anonymous referee for many helpful comments on the manuscript.

REFERENCES

1. Lynch DR, O'Neill K. Continuously deforming finite elements for the solution of parabolic problems, with and without phase change. *Int. J. Numer. Meth. Fluids*, 1981; **17**:81–96.
2. Schmidt A. Computation of three dimensional dendrites with finite elements. *J. Comput. Phys.*, 1996; **125**:293–312.
3. Gaskell PH, Savage MD, Summers JL, Thompson HM. Modelling and analysis of meniscus roll coating. *J. Fluid Mech.*, 1995; **298**:113–137.
4. Kistler SF, Schweizer PM (eds). *Liquid Film Coating*. Chapman Hall, 1997.
5. Kuiken HK. Viscous sintering: The surface-tension-driven flow of a liquid form under the influence of curvature gradients at its surface. *J. Fluid Mech.*, 1990; **214**:503–515.
6. van de Vorst GAL, Mattheij RMM, Kuiken HK. A boundary element solution for two-dimensional viscous sintering. *J. Comput. Phys.*, 1992; **100**:50–63.
7. Marar OK, Troians SM. The development of transient fingering patterns during the spreading of surfactant coated films. *Phys. Of Fluids*, 1999; **11**:3232–3246.
8. Moriarty JA, Schwartz LW, Tuck EO. Unsteady spreading of thin liquid films with small surface tension. *Physics of Fluids*, 1991; **3**:733–751.
9. Mashayek F, Ashgriz N. A spine-flux method for simulating free surface flows. *J. Comput. Phys.*, 1995; **122**:367–399.
10. Peterson RC, Jimack PK, Kelmanson MA. The solution of two-dimensional free-surface problems using automatic mesh generation. *Int. J. Numer. Meth. Fluids*, 1999; **31**:937–960.
11. Baer TA, Cairncross RA, Schunk PR, Rao RR, Sackinger PA. A finite element method for free-surface flows of incompressible fluids in three dimensions. Part I. Boundary-fitted mesh motion. *Int. J. Numer. Meth. Fluids*, 2000; **33**:375–403.
12. Soulaïmani A, Saad Y. An arbitrary Lagrangian–Eulerian finite element method for solving three-dimensional free surface flows. *Comp. Meth. Appl. Mech. Eng.*, 1998; **162**:79–106.
13. Zhou H, Derby JJ. An assessment of a parallel, finite element method for three-dimensional, moving-boundary flows driven by capillarity for simulation of viscous sintering. *Int. J. Numer. Meth. Fluids*, 2001; **36**:841–865.
14. Cerne G, Petelin S, Tiselj I. Numerical errors of the volume-of-fluid interface tracking algorithm. *Int. J. Numer. Meth. Fluids*, 2002; **38**:329–350.
15. Hirt CW, Nichols BD. Volume of fluids methods for the dynamics of free boundaries. *J. Comput. Phys.*, 1981; **39**:201–225.
16. Muttin F, Coupez T, Bellet M, Chenot JL. Lagrangian finite-element analysis of time-dependent free-surface flow using an automatic remeshing technique – application to metal casting. *Int. J. Numer. Meth. Eng.*, 1993; **36**:2001–2015.
17. Ramaswamy B, Kawahara M. Lagrangian finite-element analysis applied to viscous free-surface fluid flow. *Int. J. Numer. Meth. Fluids*, 1987; **7**:953–984.
18. Lynch DR, Gray WG. Finite element simulation of flow in deforming regions. *J. Comput. Phys.*, 1980; **36**:135–153.
19. Peterson RC, Jimack PK, Kelmanson MA. On the stability of viscous free-surface flow supported by a rotating cylinder. *Proc. R. Soc. Lond. A*, 2001; **457**:1427–1445.
20. Gresho PM, Sani RL. *Incompressible Flow and the Finite Element Method*. John Wiley, 1998.

21. Engelman MS, Sani RL, Gresho PM. The implementation of normal and/or tangential boundary conditions in finite element codes for incompressible fluid flow. *Int. J. Numer. Meth. Fluids*, 1982; **2**:225–238.
22. Schöberl J. NETGEN - An advancing front 2D/3D-mesh generator based on abstract rules. *Comput. Visual. Sci*, 1997; **1**:41–52.

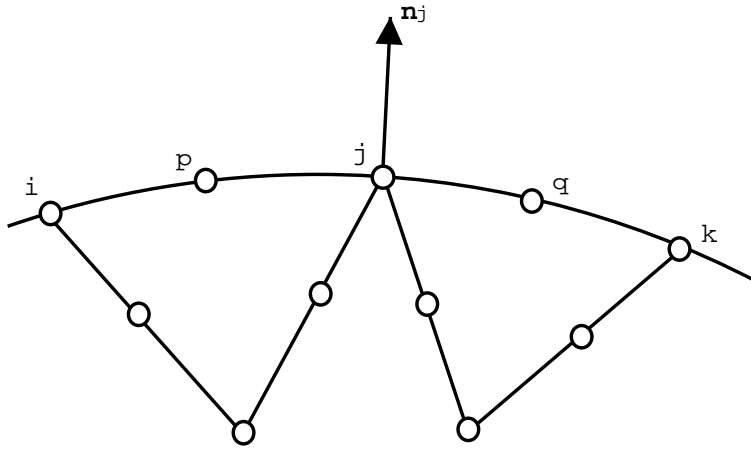


Figure 1. Isoparametric quadratic two-dimensional domain and boundary segment

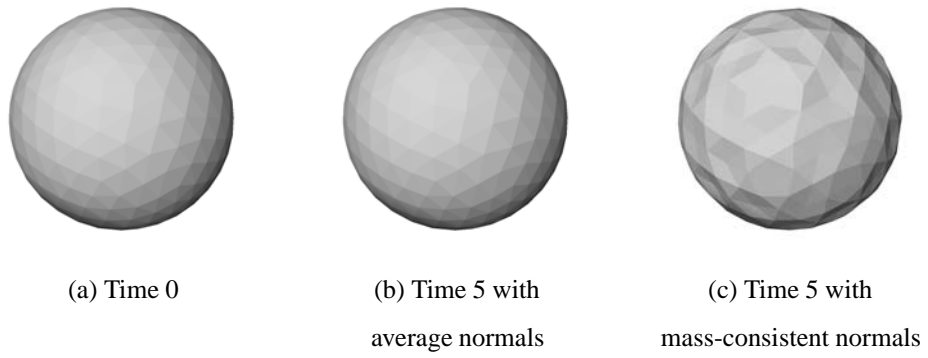


Figure 2. 3D rotating core problem. Evolution of the free surface.



(a) Time 0. $\text{Max}|u| = 0.254$ (b) Time 5. $\text{Max}|u| = 0.044$ (c) Time 10. $\text{Max}|u| = 0.013$

Figure 3. 3D perturbed free surface problem. Evolution of the free surface and maximum velocity magnitude.

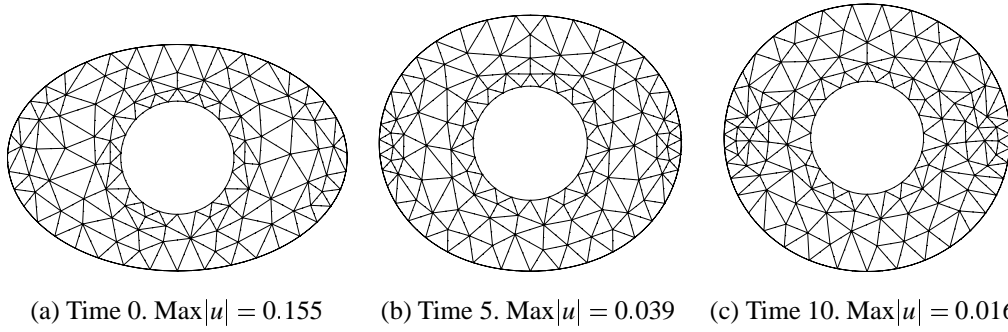


Figure 4. 2D perturbed free surface problem. Evolution of the free surface and maximum velocity magnitude.